11th ANKARA INTERNATIONAL AEROSPACE CONFERENCE **AIAC-2021-1162**
8-10 September 2021 - METU, Ankara TURKEY

INS/GNSS INTEGRATION FOR A GUIDED MUNITION WITH ERROR-STATE KALMAN FILTER

Nur Sıla Eroğlu[1] and Halil Ersin Söken[2]
Middle East Technical University
Ankara,Turkey

ABSTRACT

This study examines Inertial Navigation System (INS) and Global Navigation Satellite System (GNSS) integration with the help of error-state Kalman filter (KF) for guided munitions. Guided munitions are relatively cheap solutions for increasing the effect of the unguided bombs. They are created with the help of additional sensors to the bomb like INS and GNSS. INS and GNSS both have their advantages and disadvantages, and when these two sensors integrated, they can offer navigation results with increased accuracy. In this study, a simulation model for the guided munition is created first. Then INS/GNSS integration is achieved with the help of error-state KF equations. Finally, the filtering algorithm is adapted against the spoofing errors in the GNSS.

INTRODUCTION

The purpose of this study is applying Inertial Navigation System (INS) and Global Navigation Satellite System (GNSS) integration for a guided munition with the help of error-state Kalman filter (KF) and making the KF adaptive for cases of GNSS spoofing. For a guided munition, it is important to have precise information about the position, velocity, and attitude. In that way, the guided munition can have lower miss distance value. INS is a sensor containing both accelerometers and gyroscopes. While accelerometers are measuring the specific forces, gyroscopes are measuring the rotational velocities along the body axes of a vehicle. GNSS is a satellite-based navigation system provides pseudo-range and pseudo-range rate measurements from different satellites. With at least 4 different satellites, a vehicle with a GNSS receiver can have its own position and velocity information. INS provides navigation results in a higher frequency and higher short-term accuracy. On the other hand, GNSS provides navigation results in lower frequency and higher long-term accuracy. INS/GNSS integration make use of advantages of both sensors and eliminates the disadvantages of the sensors. INS/GNSS integration can be achieved with loosely coupled, tightly coupled or ultra-tightly coupled methods. These methods differ in measurement types for integration and the level of coupling in between the systems [Falco et al., 2017]. If pseudo range and pseudo range-rate measurements of the GNSS are converted into position and velocity measurements and integrated with INS position, and velocity measurements then it is called loosely coupled INS/GNSS integration. If pseudo range and pseudo range-rate measurements directly used in estimation with INS position and velocity measurements, then system is tightly coupled. Finally with ultra-tightly coupled method, estimated pseudo-range and pseudo range rate are fed back to the tracking loop of GNSS receiver [Noureldin et al., 2013].

[1]MSc. Student in Aerospace Engineering Department, Email: eroglu.nur@metu.edu.tr
[2] Asst. Prof. in Aerospace Engineering Department, Email: esoken@metu.edu.tr

Navigation solutions can be obtained by using different estimators such as particle filters and KF. Particle filters are advantageous in case of non-Gaussian noise distribution compared to KF which is compatible with Gaussian noise distribution case [Ko & Kim, 2012]. KF is a widely used estimator in INS/GNSS integration field. It is a two-step filter including both time update and measurement update. For the time update part, there needs to be a mathematical model of the vehicle. For the measurement update part, available measurements are fed into the filter. In KF, system and measurement noises are modelled as zero-mean known covariances [Li et al., 2010].

Different types of KF can be used as an estimator according to the needs and capabilities of the system. Linear Kalman filter cannot be used in nonlinear systems since it is an optimal estimator for linear systems. Extended Kalman filter (EKF) can be used for nonlinear systems. It linearizes the state transition matrix and observation matrix [St-Pierre & Gingras, 2004]. When the nonlinearity of the system increases, EKF can diverge or estimate badly. In that case, unscented Kalman filter (UKF) can be used. UKF uses Gaussian distribution properties and with the help of sigma points it can estimate states from set of points chosen deterministically [Vitanov & Aouf, 2014].

There are many studies about KF applications in aerospace field. Different types of KFs can be used for solving different kind of problems. In [Ohlmeyer, 2006], ultra-tightly coupled KF is used in the case of GNSS-jamming for a precision guided munition. In some KF applications, instead of using full states, error state equations are preferred by making use of small perturbation theory. Unlike full-state dynamics, error-state equations are linear and optimal KF could be achieved with this approach for an aircraft [Madyastha et al., 2011]. In [Li, 2010], adaptive extended KF is used for a land vehicle to estimate the measurement noise. According to the measurement noise, measurement matrix is manipulated. In this study, to obtain better navigation state estimates, error-state KF is applied for a guided munition. Since guided munition has short time of flight, estimation errors caused by linearization does not grow much. Error-state KF is preferred due to its lower computational-load compared to nonlinear KF algorithms.

System or measurement model can include unknown statistics and adaptive Kalman filter (AKF) can be useful to make the filter tolerant against these unknown statistics. Multiple model adaptive estimation (MMAE), covariance matching and covariance scaling methods are some ways to make a KF adaptive. In MMAE there are group of KFs with different measurement and system noise matrix values [Mohamed & Schwarz, 1998]. All KFs run at the same time and according to the obtained estimations algorithm learns which filter has the correct system and measurement covariance matrix. In covariance matching technique AKF tries to keep same theoretical and actual values of residual or innovation [Maybeck & Siouris, 1982]. Covariance scaling method is based on multiplying the covariance matrices with single or multiple scale factors calculated with respect to time [Hajiyev & Söken, 2016]. In this study, covariance scaling for measurement covariance matrix is applied to identify the errors in GNSS measurements and make KF trust less to erroneous measurements.

METHOD

6-DOF Simulation Model

For the guided munition, a 6 degree-of-freedom simulation model is created. In the model, aerodynamic forces and moments are obtained by considering the gravity, the geometry and rotation of the Earth. Accelerations and body angular rates can be obtained from the forces and moments acting on the body of the munition as follows:

$$\boldsymbol{a}_{ib}^{b} = \boldsymbol{F}^{b}/m \tag{1}$$

$$\dot{\boldsymbol{\omega}}_{ib}^{b} = \boldsymbol{I}^{b\,-1}\left(\boldsymbol{M}^{b} - \boldsymbol{\omega}_{ib}^{b} \times \boldsymbol{I}^{b}\boldsymbol{\omega}_{ib}^{b}\right) \tag{2}$$

$$\boldsymbol{\omega}_{ib}^{b} = \int \dot{\boldsymbol{\omega}}_{ib}^{b} \tag{3}$$

$$\boldsymbol{I}^b = \begin{bmatrix} I_x & -I_{xy} & -I_{zx} \\ -I_{xy} & I_y & -I_{yz} \\ -I_{zx} & -I_{yz} & I_z \end{bmatrix} \tag{4}$$

Where:

$\boldsymbol{a}_{ib}^b$: body accelerations vector resolved in body coordinate frame

$\boldsymbol{F}^b$: aerodynamical forces vector acting on the body resolved in body coordinate frame

m: mass of the munition

$\dot{\boldsymbol{\omega}}_{ib}^b$: time rate of change of body angular rates vector resolved in body coordinate frame

$\boldsymbol{I}^b$: inertia matrix resolved in body coordinate frame

$\boldsymbol{M}^b$: aerodynamical moments vector acting on the body resolved in body coordinate system

$\boldsymbol{\omega}_{ib}^b$: body angular rates vector resolved in body coordinate frame

Guidance

Proportional navigation guidance law [Shneydor, 2011] is used for creating body acceleration commands.

$$\boldsymbol{a}_{com}^n = N_{PNG} \frac{\boldsymbol{r}_{bt}^n \times \boldsymbol{v}_{bt}^n}{\boldsymbol{r}_{bt}^n . \boldsymbol{r}_{bt}^n} \times \boldsymbol{v}_{tb}^n \tag{5}$$

$$\boldsymbol{a}_{com}^b = \boldsymbol{C}_n^b \boldsymbol{a}_{com}^n - \boldsymbol{g}^b \tag{6}$$

Where:

$\boldsymbol{a}_{com}^n$: acceleration command vector resolved in navigation coordinate frame

N_{PNG}: proportional navigation guidance constant (chosen as 3)

$\boldsymbol{r}_{bt}^n$: position vector from body to target resolved in navigation coordinate frame

$\boldsymbol{v}_{bt}^n$: velocity vector from body to target resolved in navigation coordinate frame

$\boldsymbol{v}_{tb}^n$: velocity vector from target to body resolved in navigation coordinate frame

$\boldsymbol{C}_n^b$: transformation matrix from NED frame to body frame

Autopilots

Autopilots are designed for pitch, yaw and roll dynamics separately. Full state-feedback structure is used and to decrease the steady state error and an integration block is added to the system for pitch and yaw autopilots. For pitch and yaw dynamics, body acceleration is controlled. On the other hand, roll autopilot tries to make body roll angle zero. The state-feedback autopilot structure with integration block is given in Figure 1.

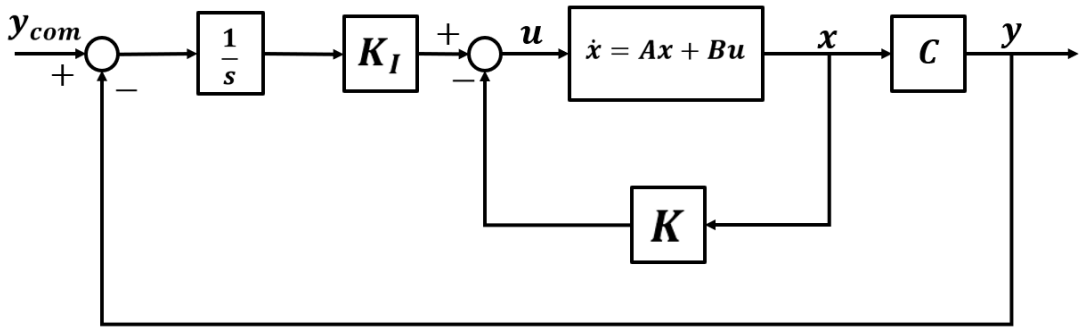

Figure 1: The State Feedback Autopilot Structure

IMU and GNSS Modeling

Body accelerations and angular velocities of the munition is obtained by using 6-DOF model. To model the IMU, bias and noise terms are added to the accelerations and angular velocities. A tactical grade IMU is chosen for this model.

$$\boldsymbol{a}_{ib}^{b,IMU} = \boldsymbol{a}_{ib}^{b} + \boldsymbol{b}_{acc} + \boldsymbol{n}_{\mathrm{acc}} \tag{7}$$

$$\boldsymbol{\omega}_{ib}^{b,IMU} = \boldsymbol{\omega}_{ib}^{b} + \boldsymbol{b}_{gyr} + \boldsymbol{n}_{gyr} \tag{8}$$

Where:

$\boldsymbol{a}_{ib}^{b,IMU}$: body accelerations vector measured by IMU resolved in body coordinate frame

$\boldsymbol{\omega}_{ib}^{b,IMU}$: body angular rates vector measured by IMU resolved in body coordinate

$\boldsymbol{b}_{acc}$: accelerometer bias vector

$\boldsymbol{b}_{gyr}$: gyroscope bias vector

$\boldsymbol{n}_{\mathrm{acc}}$: accelerometer noise vector

$\boldsymbol{n}_{gyr}$: gyroscope noise vector

In this study, GNSS modeling is achieved by using real GNSS measurements from 4 GNSS satellites, 2 GLONASS satellites and 2 GALILEO satellites. To obtain GNSS position and velocitiy estimations weighted least squares algorithm is used. GNSS measurements include pseudo range and pseudo range-rate measurements.

Equations for GNSS model is adapted from [Noureldin et al., 2013]. The difference between linearized pseudo-range measurements and estimated pseudo-range:

$$\boldsymbol{\rho}_{GNSS} - \boldsymbol{\rho}_{GNSS,est} = \frac{(x_{est} - x_{GNSS})(x - x_{est}) + (y_{est} - y_{GNSS})(y - y_{est}) + (z_{est} - z_{GNSS})(z - z_{est})}{\sqrt{(x_{est} - x_{GNSS})^2 + (y_{est} - y_{GNSS})^2 + (z_{est} - z_{GNSS})^2}} + b_r - b_r, est + \tilde{\varepsilon}_{\rho} \tag{9}$$

$$\delta\boldsymbol{\rho}_{GNSS} = \mathbf{1}_{est}^{T}\delta\boldsymbol{x} + \delta b_r + \tilde{\varepsilon}_{\rho} \tag{10}$$

Where:

$\boldsymbol{\rho}_{GNSS}$: measured pseudo-range between the satellite and the receiver

$\boldsymbol{\rho}_{GNSS,est}$: estimated pseudo-range between the satellite and the receiver

$[x \quad y \quad z]$: receiver position vector resolved in ECEF

$[x_{est} \quad y_{est} \quad z_{est}]$: estimated receiver position vector resolved in ECEF

$[x_{GNSS} \quad y_{GNSS} \quad z_{GNSS}]$: satellite position vector resolved in ECEF

b_r: errror in range due to clock bias

$b_{r,est}$: estimated error in range due to clock bias

$\tilde{\varepsilon}_{\rho}$: error in the range due to various sources

$\mathbf{1}_{est}$: estimated line-of-sight unit vector

The difference between linearized pseudo-range-rate measurements and estimated pseudo-range-rate:

$$\dot{\boldsymbol{\rho}}_{GNSS} - \dot{\boldsymbol{\rho}}_{GNSS,est} = \frac{(x_{est} - x_{GNSS})(v_x - v_{x_{est}}) + (y_{est} - y_{GNSS})\left(v_y - v_{y_{est}}\right) + (z_{est} - z_{GNSS})(v_z - v_{z_{est}})}{\sqrt{(x_{est} - x_{GNSS})^2 + \left(y_{est} - y_{GNSS}\right)^2 + (z_{est} - z_{GNSS})^2}} + d_r - d_r, est + \tilde{\boldsymbol{\varepsilon}}_{\dot{\rho}} \tag{11}$$

$$\delta\dot{\boldsymbol{\rho}}_{GNSS} = \mathbf{1}_{est}^{T}\delta\boldsymbol{x} + \delta d_r + \tilde{\varepsilon}_{\dot{\rho}} \tag{12}$$

Where:

$\boldsymbol{\rho}_{GNSS}$: measured pseudo-range-rate between the satellite and the receiver

$\boldsymbol{\rho}_{GNSS,est}$: estimated pseudo-range-rate between the satellite and the receiver

$[v_x \quad v_y \quad v_z]$: receiver velocity vector resolved in ECEF

$[v_{x_{est}} \quad v_{y_{est}} \quad v_{z_{est}}]$: estimated receiver velocity vector resolved in ECEF

d_r: errror in range-rate due to clock drift

$d_{r,est}$: estimated error in range-rate due to clock drift

$\tilde{\varepsilon}_{\dot{\rho}}$: error in the range-rate due to various sources

To solve for position and velocity estimations simultaneously, pseudo range and range-rate difference equations can be written in matrix form:

$$\begin{bmatrix} \delta\boldsymbol{\rho}^1 \\ \vdots \\ \delta\boldsymbol{\rho}^8 \\ \delta\dot{\boldsymbol{\rho}}^1 \\ \vdots \\ \delta\dot{\boldsymbol{\rho}}^8 \end{bmatrix} = \begin{bmatrix} (\mathbf{1}_{est}^1)^T & 1 & 0 & 0 \\ \vdots & \vdots & \vdots & \vdots \\ (\mathbf{1}_{est}^8)^T & 1 & 0 & 0 \\ 0 & 0 & (\mathbf{1}_{est}^1)^T & 1 \\ \vdots & \vdots & \vdots & \vdots \\ 0 & 0 & (\mathbf{1}_{est}^8)^T & 1 \end{bmatrix} \begin{bmatrix} \delta\boldsymbol{x} \\ \delta b_r \\ \delta\boldsymbol{v} \\ \delta d_r \end{bmatrix} + \begin{bmatrix} \tilde{\varepsilon}^1{}_\rho \\ \vdots \\ \tilde{\varepsilon}^8{}_\rho \\ \tilde{\varepsilon}^1{}_{\dot{\rho}} \\ \vdots \\ \tilde{\varepsilon}^8{}_{\dot{\rho}} \end{bmatrix} \tag{13}$$

$$\delta\boldsymbol{z} = \boldsymbol{G}\delta\boldsymbol{S} + \boldsymbol{\varepsilon} \tag{14}$$

Where:

$\boldsymbol{G}$: geometry matrix

The weighted least squares algorithm is as follows:

$$\delta\widehat{\boldsymbol{S}} = (\boldsymbol{G}^T\boldsymbol{R}^{-1}\boldsymbol{G})\boldsymbol{G}\boldsymbol{R}^{-1}\delta\boldsymbol{z} \tag{15}$$

$$\boldsymbol{R} = diag(\sigma_1^2 \quad \cdots \quad \sigma_n^2) \tag{16}$$

Where:

$\boldsymbol{R}$: diagonal matrice consistig standard deviations of GNSS's

Estimated states:

$$\widehat{\boldsymbol{x}} = \boldsymbol{x}_{est} + \delta\widehat{\boldsymbol{x}} \tag{17}$$

$$\hat{b} = b_{est} + \delta\hat{b} \tag{18}$$

$$\widehat{\boldsymbol{v}} = \boldsymbol{v}_{est} + \delta\widehat{\boldsymbol{v}} \tag{19}$$

$$\hat{d} = d_{est} + \delta\hat{d} \tag{20}$$

Error-State Kalman Filter

The error-state equations are given for an INS/GNSS data fusion. Before KF equations, INS mechanization equations are given in [Noureldin et al., 2013; Zhang et al., 2019]. Note that some assumptions are made here for the values too small, like values including the square of the Earth's radii.

INS Position Mechanization:

$$\delta\dot{\boldsymbol{r}}^n = \boldsymbol{F}_r\delta\boldsymbol{v}^n \tag{21}$$

$$\boldsymbol{F}_r = \begin{bmatrix} 0 & \dfrac{1}{R_M + h} & 0 \\ \dfrac{1}{(R_N + h)\cos\varphi} & 0 & 0 \\ 0 & 0 & 1 \end{bmatrix} \tag{22}$$

$$\delta\dot{\boldsymbol{r}}^n = [\delta\dot{\varphi} \quad \delta\dot{\lambda} \quad \delta\dot{h}]^T \tag{23}$$

$$\delta\boldsymbol{v}^n = [\delta v_E \quad \delta v_N \quad \delta v_U]^T \tag{24}$$

Where:
$\delta\dot{\boldsymbol{r}}^n$: time rate of change of position error vector resolved in navigation coordinate frame
$\delta\boldsymbol{v}^n$: velocity error vector resolved in navigation coordinate frame
R_N: normal radius of curvature of Earth
R_M: meridian radius of curvature of Earth
INS Velocity Mechanization:

$$\delta\dot{\boldsymbol{v}}^n = skew(\boldsymbol{f}_{ib}^n)\delta\boldsymbol{\alpha}^n + \boldsymbol{C}_b^n\delta\boldsymbol{f}_{ib}^b \tag{25}$$

$$skew(\boldsymbol{f}_{ib}^n) = \begin{bmatrix} 0 & f_U & -f_N \\ -f_U & 0 & f_E \\ f_N & -f_E & 0 \end{bmatrix} \tag{26}$$

$$\delta\boldsymbol{f}_{ib}^b = [b_{acc} \quad b_{acc} \quad b_{acc}]^T \tag{27}$$

Where:
$\delta\dot{\boldsymbol{v}}^n$: time rate of change of velocity error vector resolved in navigation coordinate frame
$\delta\boldsymbol{\alpha}^n$: attitude vector resolved in navigation coordinate frame
$\boldsymbol{f}_{ib}^n$: specific force of the body resolved in navigation coordinate frame
$\boldsymbol{b}_{acc}$: accelerometer bias
INS Attitude Mechanization:

$$\delta\dot{\boldsymbol{\alpha}}^n = \boldsymbol{F}_v\delta\boldsymbol{v}^n + \boldsymbol{C}_b^n\delta\boldsymbol{\omega}_{ib}^b \tag{28}$$

$$\boldsymbol{F}_\alpha = \begin{bmatrix} 0 & \frac{-1}{R_N + h} & 0 \\ \frac{1}{R_M + h} & 0 & 0 \\ -\frac{\tan\varphi}{R_N + h} & 0 & 0 \end{bmatrix} \tag{29}$$

$$\delta\boldsymbol{\omega}_{ib}^b = [d_{gyr} \quad d_{gyr} \quad d_{gyr}]^T \tag{30}$$

Where:
$\delta\dot{\boldsymbol{\alpha}}^n$: time rate of change of attitude vector resolved in navigation coordinate frame
d_{gyr}: drift of gyroscope

KF Time-Update:

$$\delta\hat{\boldsymbol{x}}^- = (\boldsymbol{I} + \boldsymbol{F}_k\Delta t)\delta\hat{\boldsymbol{x}}_{k-1} \tag{31}$$

$$\boldsymbol{P}_{k+1}^- = (\boldsymbol{I} + \boldsymbol{F}_k\Delta t)\boldsymbol{P}_k(\boldsymbol{I} + \boldsymbol{F}_k\Delta t)^T + \boldsymbol{Q}_k \tag{32}$$

Where:
$\delta\hat{\boldsymbol{x}}^-$: predicted error-state vector
$\boldsymbol{F}_k$: dynamic coefficient matrix
$\boldsymbol{P}_{k+1}^{-1}$: predicted covariance matrix
$\boldsymbol{Q}_k$: process noise covariance matrix

KF Measurement Update:

$$\boldsymbol{K}_k = \boldsymbol{P}_k^-\boldsymbol{H}_k^T\left(\boldsymbol{H}_k\boldsymbol{P}_k^-\boldsymbol{H}_k^T + \boldsymbol{R}_k\right)^{-1} \tag{33}$$

$$\delta\hat{\boldsymbol{x}}_k = \delta\hat{\boldsymbol{x}}_k^- + \boldsymbol{K}_k(\delta\boldsymbol{z}_k - \boldsymbol{H}_k\delta\hat{\boldsymbol{x}}_k^-) \tag{34}$$

$$\delta\boldsymbol{z}_k = \begin{bmatrix} \boldsymbol{r}_{INS} - \boldsymbol{r}_{GPS} \\ \boldsymbol{v}_{INS} - \boldsymbol{v}_{GPS} \end{bmatrix} \tag{35}$$

$$\boldsymbol{P}_k = (\boldsymbol{I} - \boldsymbol{K}_k\boldsymbol{H}_k)\boldsymbol{P}_k^- \tag{36}$$

Where:

$\boldsymbol{K}_k$: Kalman gain

$\delta\hat{\boldsymbol{x}}_k$: corrected error-state estimate vector

$\boldsymbol{P}_k$: corrected covariance matrix

$\boldsymbol{R}_k$: measurement noise covariance matrix

$\boldsymbol{H}_k$: measurement matrix

Adaptive Error-State Kalman Filter

GNSS measurmements can provide position and velocity estimations in an accurate way. However GNSS receivers can be exposed to spoofing. Spoofing is transmitting false signals so that the platform which has GNSS receiver uses as true measurements [Psiaki & Humphreys, 2016]. There are many ways to deal with these corruptions. One way is making Kalman filter adaptive. Filter can undertstand that GNSS measurements are corrupted and measurements should not be used. Since GNSS corruptions are related with measurement update part of the filter, measurement noise covariance matrix ($\boldsymbol{R_k}$) can be adapted. Filter can understand the corrupted measurement by using a statistical function $\boldsymbol{\beta_k}$ [Hajiyev & Söken, 2017]. Without the corrupted measurement the statistical function has to obey the square of normal distribution and stay below a certain threshold.In case of a faulty measurment $\boldsymbol{\beta_k}$ value increases drastically. If this value is higher than a spesific value found from chi-square table then the measurement noise covariance matrix can be adapted by using single scale factor (SSF) and multiple scale-factor (MSF) approaches [Hajiyev & Söken, 2016].

$$\beta_k = \tilde{\boldsymbol{e}}_k^T\left(\boldsymbol{H}_k\boldsymbol{P}_{k|k-1}\boldsymbol{H}_k^T + \boldsymbol{R}_k\right)^{-1}\tilde{\boldsymbol{e}}_k \quad (37)$$

$$\tilde{\boldsymbol{e}}_k = \boldsymbol{y}_k - \boldsymbol{H}_k\hat{\boldsymbol{x}}_{k|k-1} \quad (38)$$

Where:

β_k: failure detection statistical function

$\tilde{\boldsymbol{e}}_k$: innovation

SSF case:

$$S_k = \frac{\tilde{\boldsymbol{e}}_k{}^T\tilde{\boldsymbol{e}}_k - tr\{\boldsymbol{H}_k\boldsymbol{P}_{k|k-1}\boldsymbol{H}_k^T\}}{tr\{\boldsymbol{R}_k\}} \quad (39)$$

$$\boldsymbol{R}_k = S_k\boldsymbol{R}_k \quad (40)$$

Where:

S_k: scale factor value

MSF case:

$$\boldsymbol{S}_k = \left(\tilde{\boldsymbol{e}}_k\tilde{\boldsymbol{e}}_k{}^T - \boldsymbol{H}_k\boldsymbol{P}_{k|k-1}\boldsymbol{H}_k^T\right)\boldsymbol{R}_k^{-1} \quad (41)$$

$$\boldsymbol{R}_k = \boldsymbol{S}_k\boldsymbol{R}_k \quad (42)$$

Where:

$\boldsymbol{S}_k$: scale factor matrix

RESULTS

The simulation model is created, and with the help of equations of motions and the navigation results are obtained. Navigation errors will make the munition arrive at a different point then the target position. To solve this problem, INS and GNSS fusion is implemented with the help of error-state KF. The error-state KF equations will help to improve the position and velocity estimates. Note that as an example scenario the target is placed at $\boldsymbol{x}_t^n = [10000 \quad 500 \quad 0]$ m, and the munition is released from $\boldsymbol{x}_b^n = [0 \quad 0 \quad 6000]$ m.

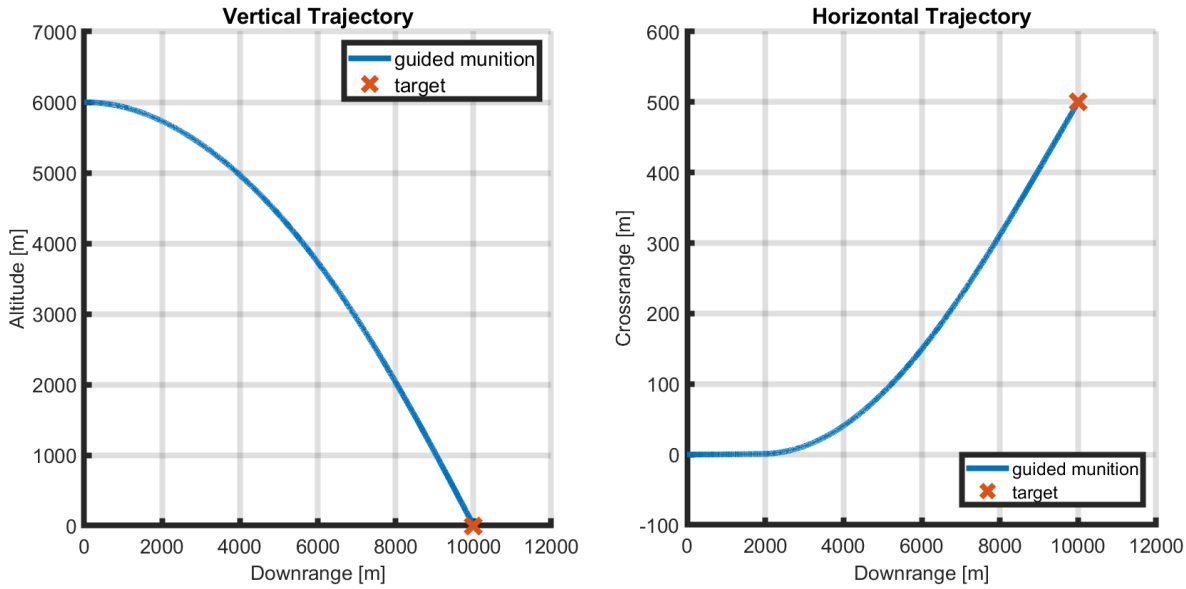

Figure 2: Guided Munition Trajectories

Figure 2 shows a no-error modelled case and guided munition can arrive at the target position succesfully. Navigation errors are calculated by finding the difference between the no-error case and KF or AKF outputs.

In this study, two different cases are examined. In the first case, INS and GNSS integration for the munition is achieved with error-state Kalman filter. In the second case, for some part of the flight the munition is exposed to GNSS spoofing and GNSS provides erroneous solution. In this situation error-state Kalman filter is modified and adapted against the spoofing errors.

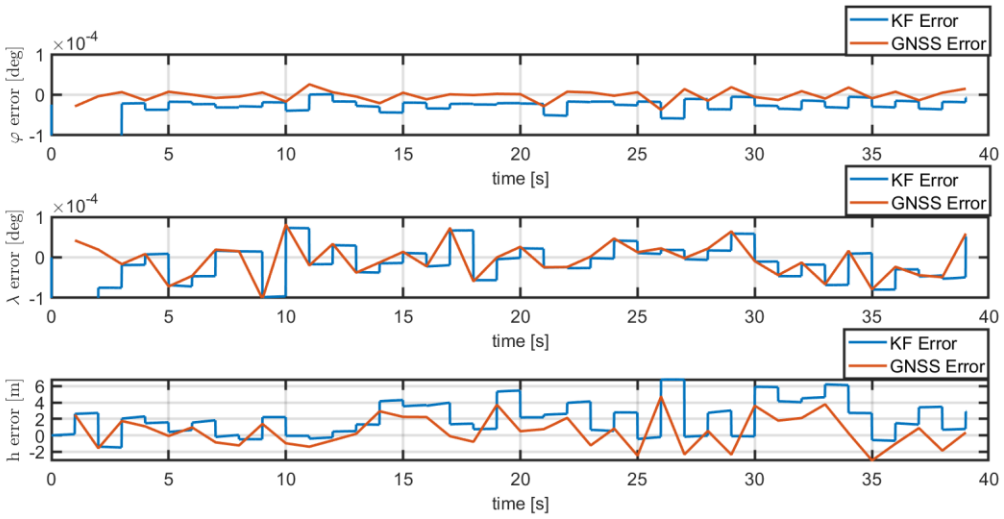

Figure 3: Position Errors for KF and GNSS

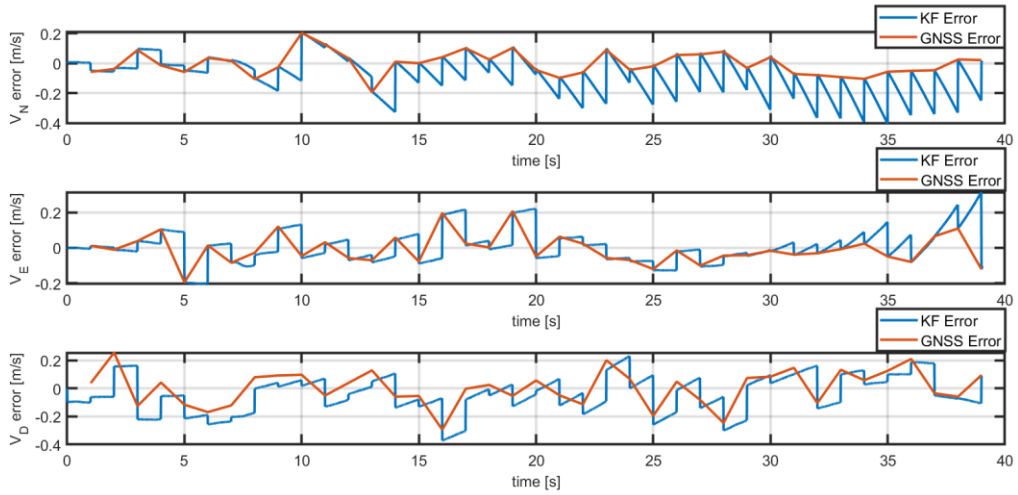

Figure 4: Velocity Errors for KF and GNSS

Figure 3 and Figure 4 illustrate the position and velocity errors obtained with KF and GNSS only. As can be observed from the Figure 3 and Figure 4, unlike INS only case; position and velocity errors are bounded. The reason of this improvement is that GNSS provides navigation solutions with more accuracy. KF make use of this accurate GNSS navigation solutions and by integrating with the INS navigation solutions more accurate, bounded and continious position and velocity solution can be obtained.

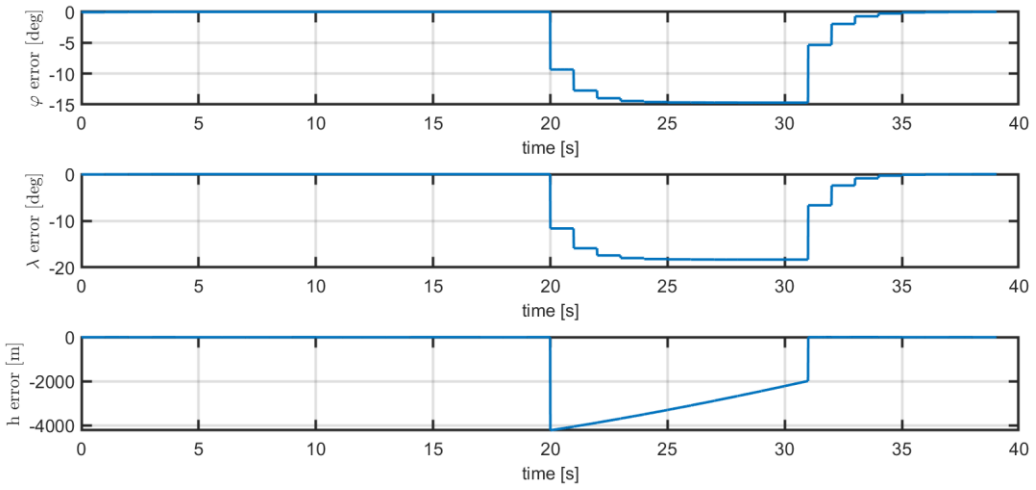

Figure 5: Position Errors In Case of GNSS Spoofing

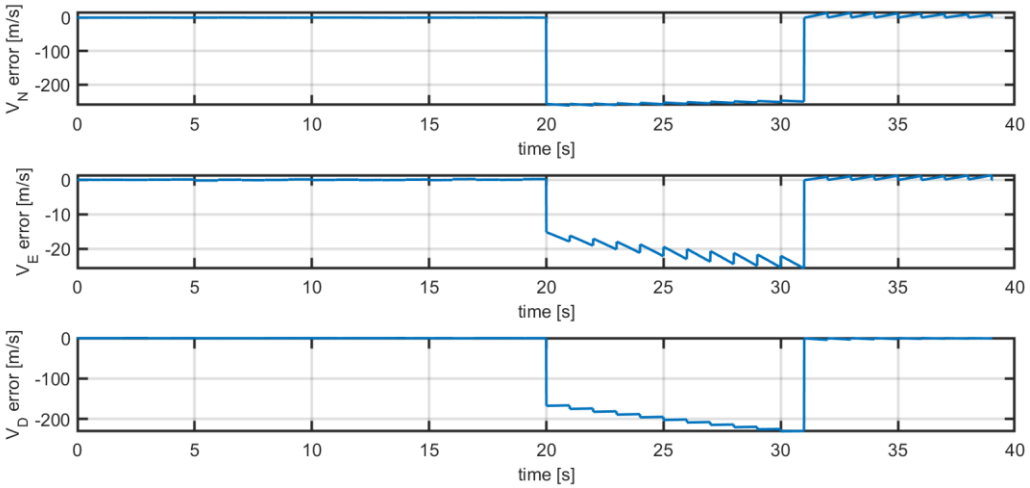

Figure 6: Velocity Errors In Case of GNSS Spoofing

Adaptive Kalman filter is applied to examine a case where GNSS results are not reliable. Figure 5 and Figure 6 demonstrate position and velocity errors in case of GNSS spoofing. During flight 10 s of GNSS spoofing is modelled. The position and velocity values obtained cannot be used, since the error between real value and estimated value is quite high. AKF implementation helps with decreasing the position and velocity errors.

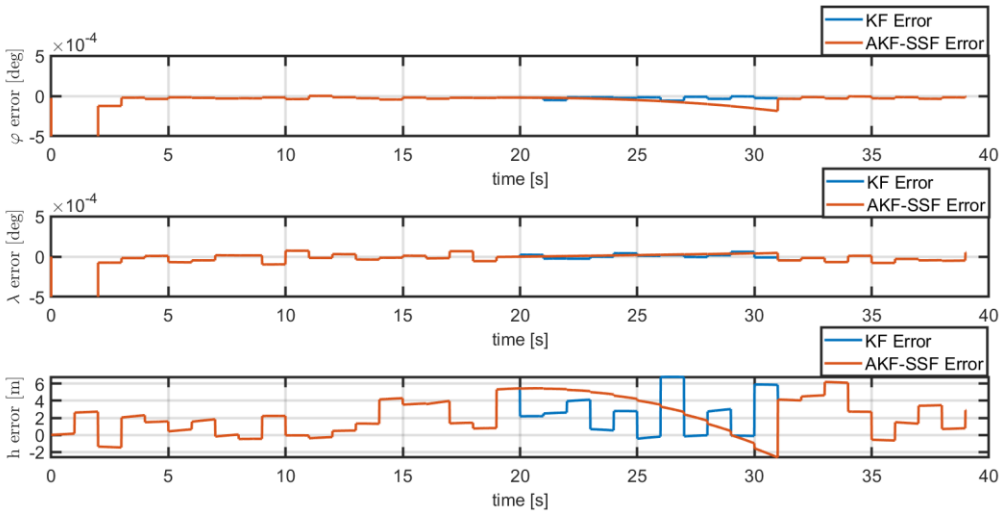

Figure 7: Position Errors Comparison

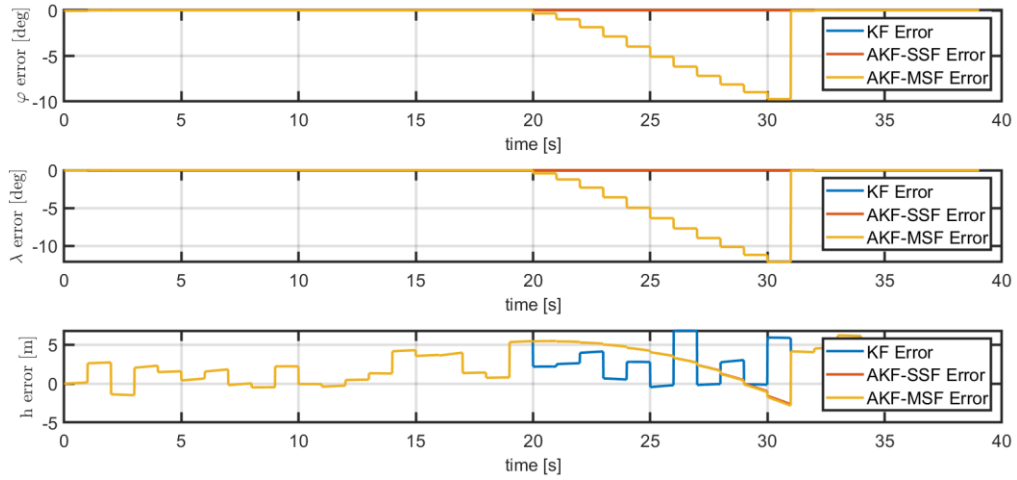

Figure 8: Position Errors Comparison

In Figure 7, KF position errors without GNSS spoofing and AKF with SSF with GNSS spoofing are given. Even though there is an increase in position errors, compared to the Figure 5, position errors decreased a lot. When the AKF is not used, maximum latitude error is 15°, maximum longitude error is 20° and maximum altitude error is 4000 m. However with SSF-AKF all position errors are very close to those for no-GNSS spoofing case. Figure 8 shows additionally AKF with MSF. Position errors with MSF-AKF are less than no adaptive case however more than those for the SSF-AKF.

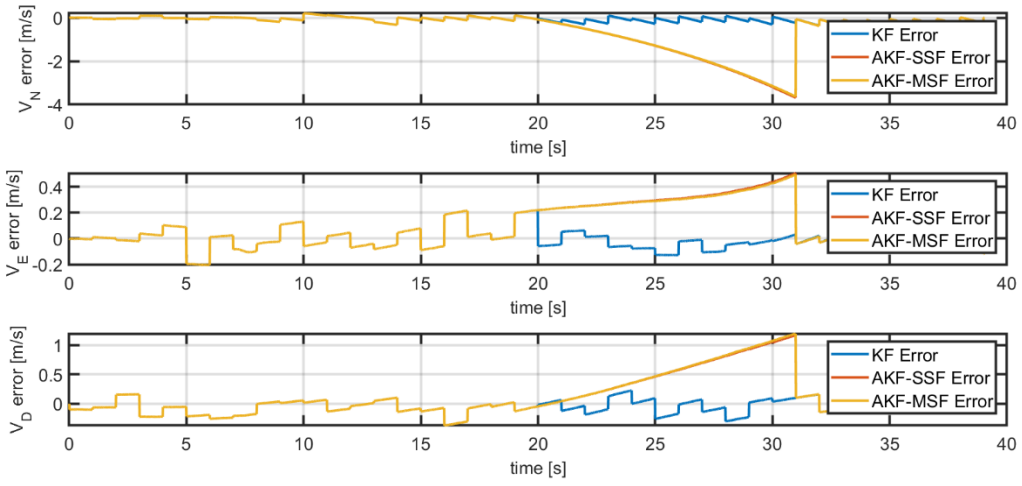

Figure 9: Velocity Errors Comparison

Figure 9 interprets the velocity errors with no-GNSS spoofing case and SSF-KF and MSF-KF with GNSS spoofing case. Compared to the Figure 6, which velocity errors reaches 200 m/s with the adaptation of KF velocity errors decrease to 4 m/s. Velocity errors of MSF-AKF is slightly less than SSF-AKF.

CONCLUSION

This study aims to represent an application of KF for a guided munition to have improved navigation solutions. KF application is achieved for INS/GNSS integration and AKF application succeeded to have better navigation solution in case of GNSS spoofing. For AKF, two different methods are investigated which are SSF-AKF and MSF-AKF. Both of these methods work for decreasing the errors in navigation solutions. SSF-AKF has much lower position errors compared to MSF-AKF. On the other hand, MSF-AKF has slightly lower velocity errors compared to SSF-AKF. According to the need of the air vehicle applied one of the AKF methods can be chosen. In this scenario of the guided munition SSF-KF seems to be more advantageous. However, to choose the appropriate method for guided munition more analysis should be done.

References

Falco, G., Pini, M., & Marucco, G. (2017) *Loose and Tight GNSS/INS Integrations: Comparison of Performance Assessed in Real Urban Scenarios*, Sensors, Vol 17(2), p: 255-279

Hajiyev, C., & Soken, H. E. (2016) *Fault Tolerant Estimation of UAV Dynamics via Robust Adaptive Kalman Filter*, Complex Systems, p: 369–394

Ko, N. Y., & Kim, T. G. (2012) *Comparison of Kalman filter and particle filter used for localization of an underwater vehicle*, 2012 9th International Conference on Ubiquitous Robots and Ambient Intelligence (URAI), Nov 2012

Li, B., Cai, L., & Xiao, M. (2010) *Adaptive Extended Kalman Filtering Algorithm for SINS/GNSS Integrated Navigation in guided munitions.* 2010 IEEE International Conference on Intelligent Computing and Intelligent Systems, Aug 2010

Madyastha, V., Ravindra, V., Mallikarjunan, S., & Goyal, A. (2011) *Extended Kalman Filter vs. error State Kalman Filter for aircraft Attitude Estimation,* AIAA Guidance, Navigation, and Control Conference, Aug 2011

Maybeck, P. S., & Siouris, G. M. (1980) *Stochastic Models,* Estimation, and Control, Volume I. IEEE Transactions on Systems, Man, and Cybernetics, Vol 10(5), p: 282–282.

Mohamed, A. H., & Schwarz, K. P. (1999) *Adaptive Kalman Filtering for INS/GPS,* Journal of Geodesy, Vol *73*(4), p: 193–203

Noureldin, A., Karamat, T. B., & Georgy, J. (2013) *Fundamentals of inertial navigation, satellite positioning and their integration*, Heidelberg: Springer

Ohlmeyer, E. (2006) *Analysis of an ultra-tightly coupled GNSS/ins system in jamming,* 2006 IEEE/ION Position, Location, And Navigation Symposium, Jan 2006

Psiaki, M. L., & Humphreys, T. E. (2016) *GNSS spoofing and detection,* Proceedings of the IEEE, Vol 104(6), p: 1258–1270

Shneydor, N. A. (2011) *Missile guidance and pursuit: Kinematics, dynamics and control,* Cambridge, UK: Woodhead Pub

St-Pierre, M., & Gingras, D. (2004) *Comparison between the unscented kalman filter and the extended kalman filter for the position estimation module of an integrated navigation information system,* IEEE Intelligent Vehicles Symposium, Jun 2004

Vitanov, I., & Aouf, N. (2014) *Fault diagnosis for MEMS INS using unscented Kalman filter enhanced by Gaussian process adaptation,* 2014 NASA/ESA Conference on Adaptive Hardware and Systems (AHS), Jul 2014

Zhang, M., Li, K., Hu, B., & Meng, C. (2019) *Comparison of Kalman filters for Inertial integrated navigation* Sensors, Vol 19(6), p: 1426-1451